The mid-8th century CE surface faulting along the Dead Sea Fault at Tiberias (Sea of Galilee, Israel)

M. F. Ferrario[1], O. Katz[2], A. Hillman[3], F. Livio[1], R. Amit[2] and A. M. Michetti[1]

[1] Università degli Studi dell'Insubria, via Valleggio 11, 22100 Como, Italy.

[2] Geological Survey of Israel, 30 Malkhe Israel Street, 95501 Jerusalem, Israel

[3] Israel Antiquities Authority.

Corresponding author: Maria Francesca Ferrario (francesca.ferrario@uninsubria.it)

Key Points:

- We describe evidence of surface faulting as recorded in archaeological relics at the ancient Tiberias (Israel)
- We attribute this faulting to one of the earthquakes occurred during the mid-8th century CE
- Our findings highlight the need for revising the seismic risk in the Sea of Galilee and nearby regions.

Abstract

The Dead Sea Fault (DSF) is a plate-boundary where large earthquakes are expected and largely overdue. Complex sequences of earthquakes along the DSF are documented by historical evidence, one of the most devastating being in the mid-8th century CE. Nevertheless, the related seismogenic sources are still debated. Here we describe site-specific archaeoseismological observations at the ancient Tiberias city, located on the western shore of the Sea of Galilee. We map Roman and Byzantine relics faulted in the mid-8th century CE by a pure dip-slip normal fault. We use geophysical, geomorphological and structural analyses integrated with published data, to assess the seismic hazard of the Jordan Valley Western Boundary Fault (JVWB). We propose that the normal JVWB can rupture the surface along its ~45 km trace running from Tiberias toward the S crossing Beit Shean, Tel Rehov and Tel Teomim. The JVWB, parallel to the main strike-slip Jordan Valley Fault segment, might be regarded as a major earthquake source in this region. We test the hypotheses of both single fault and multi-faults rupture scenarios, which result in an expected range of Mw from 6.9 (single rupture of the JVWB) to 7.6 (multiple rupture of the JVWB and Jordan Valley Fault). Our results suggest that seismic source characterization in the Sea of Galilee region must include normal faults capable of surface rupturing, despite the absence of such events in the instrumental catalogue.

KEYWORDS

Dead Sea Fault; mid-8th century CE seismicity; Tiberias; archaeoseismology; seismic hazard; strain partitioning

1 Introduction

The spatial and temporal characterization of faults rupture, the expected magnitude range, fault dimension, focal mechanism and affected areas are primary parameters for the evaluation of the seismic risk of a region. The time interval covered by instrumental seismicity can be too short to have witnessed strong earthquakes, if these have recurrence intervals longer than ca. 100 years. It is therefore vital to extend the time window covered by instrumental catalogues, using historical records, archaeoseismological and paleoseismological evidences (e.g., Bozorgnia & Bertero, 2004). These techniques provide valuable information to investigate past events with long recurrence intervals, however a gross overestimation of the size of historical earthquakes can occur if the combined effects of multiple individual events are attributed, over the years, to a single earthquake (Ambraseys, 2005).

In this study we focus our investigations on the Sea of Galilee region (Israel), located along the Dead Sea Fault (DSF). The study area is particularly suitable for an archaeoseismological approach because it has a long-lasting human occupation and over 150 years of extensive archeological excavations provide abundant relics pertaining to different historical periods. Strong earthquakes are known to have hit the Sea of Galilee area in historical times (e.g. Ambraseys, 2005, 2009; Guidoboni et al., 2007), but the instrumental catalogue is limited to $M < 6$ earthquakes (recorded events since the first half of the 20th century). A seismic swarm (max Mw 4.5) occurred in July-August 2018, with epicenters located in the NW part of the Sea of Galilee (Wetzler et al., 2019), renewing the interest for seismic risk evaluation in the area.

In this study, we systematically document archaeoseismological evidence indicating normal surface faulting at the city of Tiberias, located on the W shores of the Sea of Galilee (Section 4.1), then we use morphotectonic data and newly acquired shallow geophysical prospection (Section 4.2) to characterize this normal fault. Based on the new observations, we relate the damage to the mid-8th century CE seismicity (Section 5.1) and discuss the structural setting and fault displacement hazard at Tiberias (Section 5.2) taking into account single and multi-faults rupturing scenarios (Section 5.3). Our data allow to: i) assess the kinematics and characteristics of the earthquake which generated the surface faulting at Tiberias during the mid-8th century CE, ii) define the trace, kinematics and latest movement of an active fault crossing through the modern town of Tiberias and iii) highlight the need to consider several rupture scenarios for a comprehensive seismic risk assessment of the Sea of Galilee region.

2 Study area and literature review

2.1 Structural and geologic setting

The DSF (Fig. 1a) forms the boundary between Arabia and Sinai plates and accommodates a long-term slip rate of about 4 – 5 mm/yr, resulting in 105 km of post-Miocene left-lateral displacement (e.g., Garfunkel, 1981; Garfunkel et al., 2014 and references therein). In the Sea of Galilee area, the main fault segment is the left-lateral Jordan Valley Fault (JVF), which runs along the E side of the Sea of Galilee (Marco et al., 2005; Hamiel et al., 2016; Wechsler et al., 2018 and reference therein; Fig. 1b). The JVF is characterized by Holocene left-lateral and normal components, which are estimated to be 4 - 5 mm/yr and 0.1 - 0.2 mm/yr respectively, based on paleoseismology (Ferry et al., 2007; Katz et al., 2010) and on GPS data.

The latter indicates shallow creep behavior of the JVF along the SE coast of the Sea of Galilee (Hamiel et al., 2016).

The SW coast of the Sea of Galilee is crosscut by a series of mostly E-dipping normal faults (Fig. 1c; Sneh, 2008; Sneh and Weinberger, 2014; Sagy et al., 2016; Sharon et al., 2020). North of Tiberias, these faults bend westward and assume an E-W trending (Fig. 1b, c). Southward these faults join in a single trace, that is discontinuously traced until Bet Shean toward Tel Rehov and Tel Teomim, at the intersection with the the Carmel – Gilboa Fault. It is still debated whether the JVF and the normal faults at the W side of the Sea of Galilee presently accommodate the relative plate motion according to a strain-partitioned model (e.g., Garfunkel, 1981; Ben-Avraham & Zoback, 1992; Sagy et al., 2003), and thus might be regarded as individual seismic sources or, conversely, the Sea of Galilee is a pull-apart basin (e.g., Hurwitz et al., 2002) dissected on the western side by secondary normal faulting.

Previous studies investigated the W side of the Sea of Galilee at several sites through geophysical prospecting (Fig. 1b; Rotstein et al., 1992; ten Brink et al., 1999; Hurwitz et al., 2002; Sneh and Weinberger, 2014). Constraints on the fault location are provided by the Hamat Tiberias hotsprings (Fig. 2a), interpreted as linked to a steep E-dipping normal fault (Ilani et al., 2006). Further S, geomorphic and structural evidence is used by Sagy et al. (2016) to map a series of active normal fault segments for a total length of 40 - 45 km up to Tel Rehov and Tel Teomim, where Late Pleistocene normal faulting has been described in detail by trenching (Fig. 1b; Zilbermann et al., 2004; Sagy et al., 2016). Field mapping, offset landforms and exploratory excavations allow to estimate the Quaternary normal slip rate of this fault in 0.5 – 2 mm/yr, without significant strike-slip component (Zilbermann et al., 2004; Eppelbaum et al., 2007). In the following, we refer to the whole segment from Tiberias to Tel Rehov and Tel Teomim as the Jordan Valley Western Boundary Fault (JVWB), and for modelling purposes we assume that it is continuous at the sub-surface.

We focus our investigations on the W side of the Sea of Galilee, in the southern outskirts of the modern town of Tiberias. The stratigraphic setting of the escarpment bounding the Sea of Galilee to the W (Fig. 1c) is characterized by a Plio-Pleistocene basaltic plateau which overlie Cretaceous limestones, occasionally outcropping, and Neogene-Quaternary basin infillings. Well-developed triangular facets and wineglass-shaped valley outlets, fluvial elbows and piracy events point to a tectonic origin for the range front residing along the JVWB (Fig. 2).

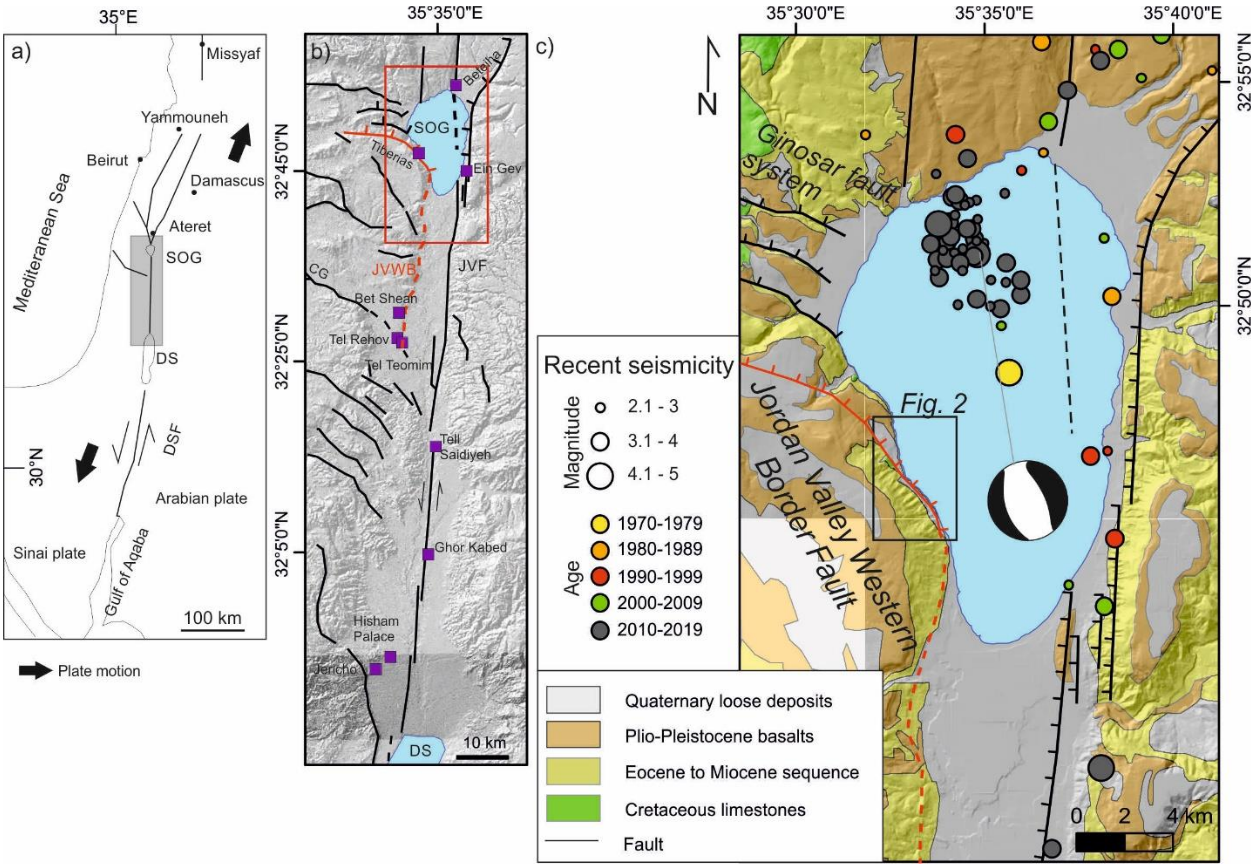

Figure 1. *Structural framework of the Tiberias area; a) plate tectonic setting of the Dead Sea Fault (DSF), the grey box locates the area shown in (b), between the Sea of Galilee (SOG) and the Dead Sea (DS); b) Quaternary faults in the central part of the DSF, modified after Sneh and Weinberger (2014), Sagy et al. (2016), Hamiel et al. (2016) and Sharon et al. (2018, 2020); the red rectangle is the area enlarged in c); JVWB: Jordan Valley Western Boundary Fault, JVF: Jordan Valley Fault, CG: Carmel-Gilboa Fault; c) simplified geologic map (after Bogoch & Sneh, 2008; Sneh, 2008), epicenters of Mw > 3.0 events since 1980 (data from http://seis.gii.co.il/en/earthquake/searchEQSRslt.php) and focal mechanism of the 2018 Mw 4.5 event (after Wetzler et al., 2019).*

2.2 Historical evolution and investigated sites at Tiberias

The Roman city of Tiberias was founded in the name of Emperor Tiberius by Herod Antipas in 19 CE. Archaeological excavations carried out at Tiberias reported abundant earthquake-related damage in archeological strata (Hirschfeld & Meir, 2004; Hirschfeld & Gutfeld, 2008; Zingboym & Hartal, 2011; Dalali-Amos, 2016; Onn & Weksler-Bdolah, 2016). We performed our investigations at three sites (namely the Theatre, the Southern Gate and a water reservoir), now at the southern part of the modern city (Fig. 2a).

Atrash (2010), reconstructed three building phases in the Theatre. These phases contribute to the analysis of the earthquake effects (Fig. 3a): during the earliest building phase (Stratum V, 1st century CE), the Theatre was smaller and had two blocks of seats; in the second phase (Stratum IV, 2nd-3rd century CE) a third block of seats and a larger *auditorium* were added.

In the third phase (Stratum III, 4th-6th century CE), the third block of seats was dismantled and a tribune was added. In the 6th-7th century CE, the Theatre has been downscaled and then abandoned, as testified by debris flow deposits that buried the site. Finally, a Fatimid-Abassid residential quarter (Strata I-II, 8th-11th century CE) was built on the Theatre remains and was in use until late 11th century CE (Atrash, 2010). The Fatimid-Abassid structures were completely removed during the excavation (2009); the present-day status of the site is shown in Fig. 4, together with the view angle of photos taken during our surveys (2014-2015), whereas those taken during the 2009 excavations are shown in Fig. 5.

The Southern Gate, located ca. 200 m S of the Theatre, was originally built during the Early Roman period as a free-standing structure. In Byzantine times, the gate was incorporated in the newly-built city wall and in Umayyad-to-Fatimid periods other buildings and retaining walls were constructed at the site (Hartal et al., 2010). Between the Theatre and Southern Gate, an Umayyad water reservoir was uncovered in 2017 (Fig. 6a).

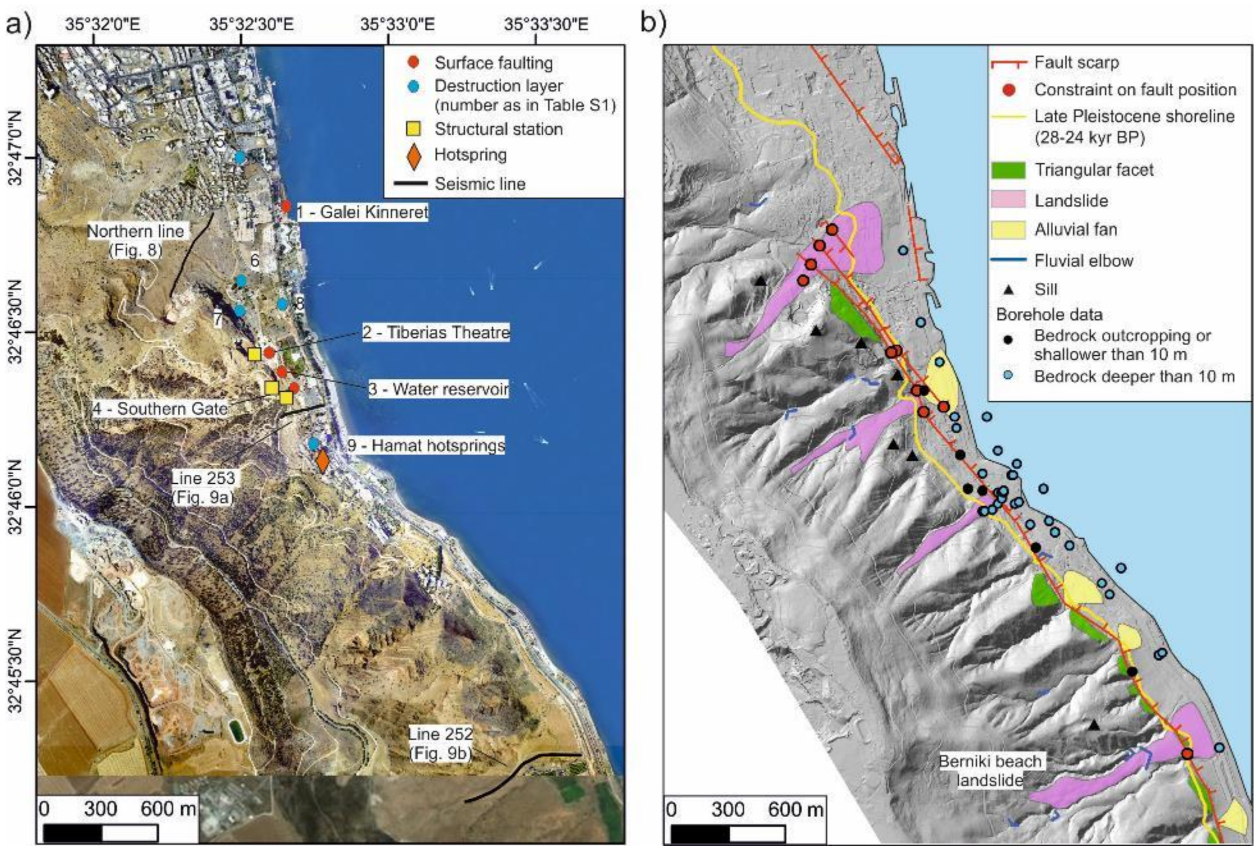

***Figure 2**. a) Relevant sites mentioned in the text and location of the seismic lines; numbers correspond to Table S1 where relevant references are provided; b) Morphotectonic map of the study area, based on 0.5-m resolution DTM extracted from airborne Lidar survey. The map shows also the late-Pleistocene shoreline, the position of boreholes analyzed in this study and the points where we constrained the spatial position of the fault trace.*

a)

Historical periods in Israel	Age (cent. CE)	Stratum (Theatre)
Fatimid - Abassid	8 - 11th	I - II
Umayyad	7 - 8th	not present
Byzantine	4 - 6th	III
Middle/Late Roman	2 - 3rd	IV
Early Roman	1st	V

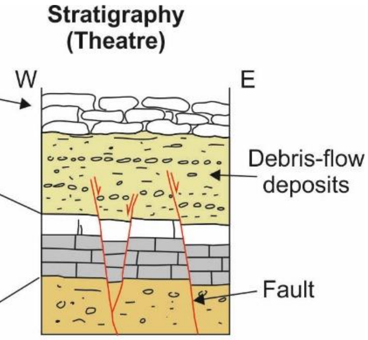

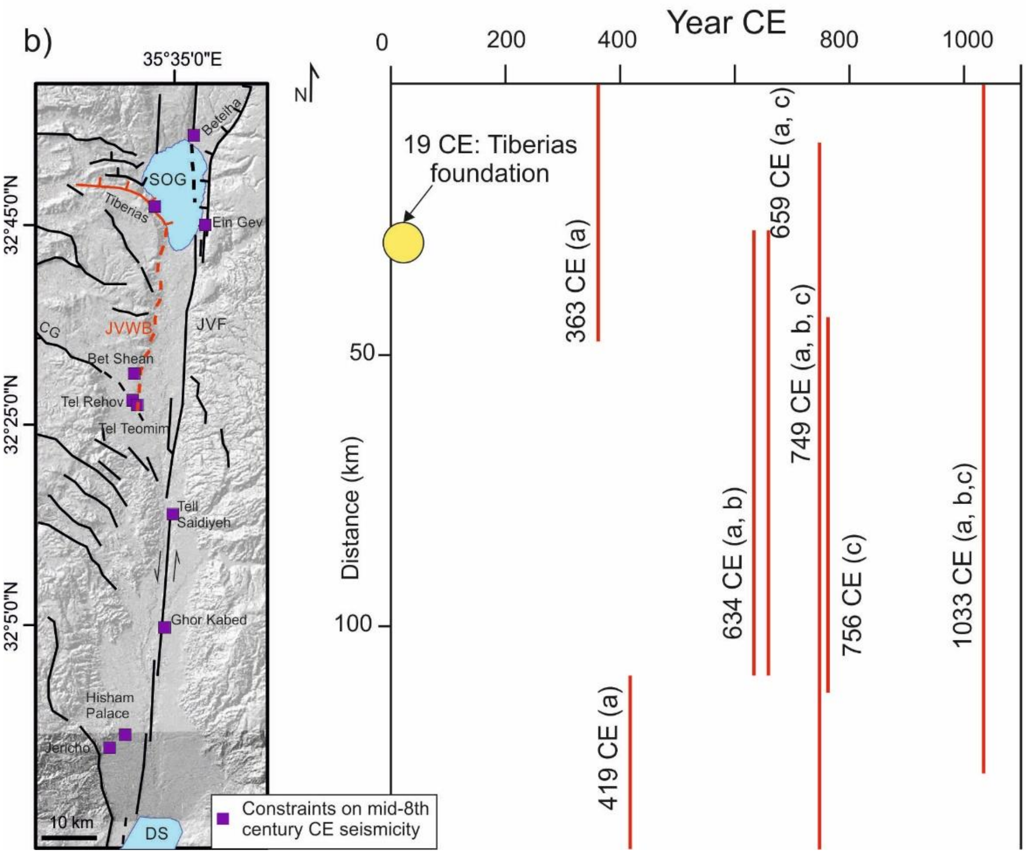

***Figure 3**. a) Historical periods in Israel and schematic stratigraphic column at the Theatre; b) Spatial and temporal distribution of the major documented earthquakes (estimated magnitude above ca. 6) that affected the Jordan Valley between Tiberias foundation at 1st century CE and the 11th century CE. Data are from published literature, indicated by the letters in brackets; a: Agnon (2014), b: Marco & Klinger (2014) and c: Zohar (2019). Vertical bars represent the presumed spatial extent of ruptures relative to the faults map.*

2.3 Historical seismicity

Information on past earthquakes along the DSF is particularly rich and includes evidence for strong but infrequent earthquakes derived from historical, archaeological and geological data (Guidoboni et al., 2007; Ambraseys, 2009; Agnon, 2014; Zohar et al., 2016). Here we limit our description to the region between the Sea of Galilee and the Dead Sea. For a thorough review of the historical seismicity along the entire DSF and related paleo- and archaeoseismological evidence, the reader is referred to the several review papers published on this topic (e.g., Guidoboni et al., 2007; Ambraseys, 2009; Agnon, 2014; Garfunkel et al., 2014; Marco & Klinger, 2014; Zohar et al., 2016; Zohar, 2019). An integration of data from recent seismology, historical, archeological and paleoseismological investigations revealed that the recurrence interval in Sea of Galilee region is about 500 and 1500 years for earthquakes of Mw > 6 and Mw > 6.5, respectively (Ambraseys, 2009; Hamiel et al., 2009; Katz et al., 2010). Such large earthquakes may generate ground acceleration up to 0.5g and earthquake-induced landslides around the Sea of Galilee (Katz et al., 2010).

Fig. 3b summarizes the earthquakes occurred in the studied region since Tiberias foundation (1st century CE) and the 11th century CE. In the following, we provide more details on the mid-8th century CE seismicity, the most relevant for our study. During this period, a sequence of strong earthquakes spatially and temporarily clustered occurred along the DSF. They were felt over a large area extending between N Syria and Egypt, but the amalgamation of literary information (e.g., Karcz, 2004; Ambraseys, 2005, 2009) resulted in an unlikely image of damaging produced by a single event (i.e., estimated Mw 7.0-7.5; Marco et al., 2003). Teophanes, one of the reliable and most-contemporary sources, mentions instead three distinct earthquakes between 747 and 757 CE (Ambraseys, 2005). The precise dating of the events is debated, although numismatic indications constrain destruction at Bet Shean (Scythopolis), located along the southern part of the JVWB (Fig. 3b), after than August 748 CE (Tsafrir & Foerster, 1992; Karcz, 2004).

Several authors dealt with the mid-8th century CE seismicity, based on archaeological, paleoseismic and macroseismic studies. Starting from the N, paleoseismic evidence matching this time frame was found along the Missyaf (Meghraoui et al., 2003) and Yammouneh (Daeron et al., 2007) Faults (Fig. 1a). At Galei Kinneret, about 1.5 km N of the Theatre (Fig. 2a), Marco et al. (2003) documented secondary E-dipping normal faults dated as late as the early 8th century CE, whereas buildings from the late 8th century CE were intact. Along the JVF (Fig. 1b), paleoseismic surface ruptures related to the same event were found at Beteiha (Wechsler et al., 2018), Ein Gev (Katz et al., 2010), Tell Saidiyeh and Ghor Kabed (Ferry et al., 2007). At Hisham Palace (Jericho), Reches & Hoexter (1981) documented surface faulting as well. Damage at this site has been re-assessed as due to the 1033 CE earthquake (Alfonsi et al., 2013), but the latter study did not address the main fault strand, thus a mid-8th century event cannot be definitely excluded. South of the Dead Sea, a rupture matching the mid-8th century CE interval and extending to the Gulf of Aqaba (Fig. 1a) is inferred by Agnon (2014) using macroseismic and archaeological evidence and by Lefevre et al. (2018) using paleoseismological investigations.

2.4 Recent seismicity

The instrumental catalogue (http://seis.gii.co.il/en/earthquake/searchEQS.php) includes 77 earthquakes with Mw > 2.5 in the area depicted in Fig. 1c since 1970, 4 of which had Mw > 4.0. These include a Mw 4.0 occurred in 2011 along the JVF and 3 events with epicenter offshore in the Sea of Galilee (Fig. 1c). The oldest one in the catalogue (Mw 4.2) occurred in 1972, whereas the 2 most recent (Mw 4.5 and 4.2) occurred in July 2018 as part of a swarm of shallow earthquakes with normal focal mechanism solutions (focal depth < 10 km). Seismicity is located offshore, in the NW part of the Sea of Galilee, aligned along NNW-SSE direction (Wetzler et al., 2019).

3 Materials and methods

3.1 Morphotectonics

We use high resolution airborne-Lidar based topographical model, acquired for the entire Sea of Galilee coastal area by Ofek Aerial Photo, using Optech ORION H300 (covered area: over 150 km^2). Products include ground-validated DSM and DTM with pixel size of 0.5 m x 0.5 m and average vertical error of less than 10 cm. We process the data obtaining maps of slope, aspect and contour lines. We interpret multiscale aerial photos (two coverages imaging the area at 1945 and 1982) using an analogic stereoscope.

We map linear and areal features with a clear geomorphic expression at the surface (i.e., abrupt change in topography and slope) and discriminate tectonic from lacustrine features (e.g., late Pleistocene shorelines, Hazan et al., 2005) and man-made structures using Lidar data and high spatial resolution satellite images (Esri imagery). We check available borehole logs at the Geological Survey of Israel archives, providing additional data on the shallow subsurface. We implement information in a GIS database and finally we directly study the mapped elements through field reconnaissance. We draw geologic cross-sections at three key sites, using surface (fieldwork, Lidar and aerial imagery interpretation) and shallow subsurface (seismic lines and borehole logs) constraints.

We consider the mapped faults as highly reliable due to at least one of the following reasons: (i) were directly observed at the archaeological sites, (ii) investigated through seismic lines, (iii) deducted from borehole logs, (iv) mapped in the official Israeli active fault map (Sagy et al., 2016), (v) described in detail in scientific literature (e.g., Marco et al., 2003).

3.2 Archaeoseismology and structural analysis

We surveyed Tiberias Theatre and the Southern Gate in 2014-2015. Archaeological stratigraphy enabled to date the relics and related damage. We acquire about 30 high-resolution low-aerial photographs from different perspectives and heights using a DJI Phantom drone.

We classify Earthquake Archaeological Effects (EAE) according to type (fractures on ground or on walls, folded walls, chip corners), following the guidelines provided by Rodriguez-Pascua et al. (2011). Damage was mapped on a high-resolution image acquired by a UAV-airborne camera. We measure structural data (dip and dip direction) on 182 fractures within the archaeological sites (see Table S2) using a compass or an Android mobile equipped with FieldMove CLINO app by Midland Valley®, and we plot data using Stereonet v.7 software by Rick Allmendinger. We measure a set of 15 well-constrained faults with kinematic indicators on the outcropping bedrock at 3 different stations between the Theatre and the Gate (raw data are listed in Table S3). We invert for slip with the software FaultKin v.6 (Allmendinger et al., 2001), following a kinematic approach (i.e., Unweighted Moment Tensor Solution) in order to derive strain axes from fault geometry and slip direction. This method assumes that slip direction on fault is parallel to the maximum resolved shear rate of a large-scale homogeneous strain rate tensor (e.g., Marrett & Allmendinger, 1990).

We carry high resolution topographic surveys using a total station (Sokkia; SET3R), focused on seat courses and wall stones, considered as an originally horizontal datum, in order to measure faults vertical displacement with cm-scale accuracy. We carefully selected the location of the profiles, in order to keep original elements, not replaced during the restoration process.

3.3 Seismic survey

For the purpose of this study three high resolution seismic reflection profiles were acquired by the Geophysical Institute of Israel to image the shallow subsurface of the faults recognized at Tiberias Theatre and the Southern Gate (see Section 4.2). Lines were placed in order to intercept morphologic lineaments interpreted as possibly connected to active tectonics, avoiding restricted or inaccessible areas.

The first two lines are located close to the Southern Gate (Line 253) and at Berniki Beach landslide (Line 252), i.e., 2.5 km S of Tiberias Theatre (Fig. 2a). The following parameters are used: 500 mSec record length, 0.5 mSec sample rate, 2.5 or 5 m shot intervals using 48 channels (Medvedev, 2008). The energy source is a Digipulse and the recorder is a Strata View RX-60. For the third line, located N of Tiberias Theatre (Northern Line; Fig. 2), high density data are collected using a 2 Sec record length and 1 mSec sample rate. The line included 201 channels in 2.5 m intervals. A reflection survey with a tomography approach has also been conducted. The data is recorded using a Geometrics Geode system and Oyo Geospace GS-32CT 10 Hz Geophones. The seismic source wavelet is generated by a M27 HR truck mounted vibroseis. Data are processed using the Landmark® (ProMax) software; optimal signal/noise ratio is obtained through noise attenuation and band-pass filtering. Data visualization and interpretation is realized using SeiSee software, and is based on reflectors dip and continuity, whereas lines were drawn through commercial graphic software. Further details on the processing steps are provided in Text S1.

4 Results

4.1 Archaeoseismological observations

4.1.1 Evidence for surface faulting: the Tiberias Theatre and the Southern Gate

Cretaceous limestones outcrop in the NW side of the Theatre (Fig. 4a), while the E side lies on loose alluvial deposits. At the contact, a bedrock fault zone (N60/60) is exposed inside the Theatre as a 1.5 m thick fault gouge (Fig. 4e). Stress inversion of fault slip data (Fig. 4d and Table S3) indicates an almost pure extensional regime, with a T axis trending N62/13. The limestone – alluvial deposit contact has a clear morphological expression out of the Theatre area (i.e., lies at the base of the mountain escarpment) and is interpreted as tectonic in origin on the Israeli map of active faults (Sagy et al., 2016).

The Theatre preserves evidence of damage (Fig. 4a), mainly aligned along a ca. 10 m wide, N140-trending, belt which is located ca. 30 m to the E of the bedrock fault gouge described above. These archaeoseismic effects include on-fault effects with vertical displacement (downthrown seat-rows and walls) and strain structures generated by permanent ground deformation (tilted and folded walls). All these features belong to the primary earthquake archaeological effects described by Rodriguez-Pascua et al. (2011). The most relevant evidence is a 5-m wide, at least 15 m long, coseismic gravity-graben affecting the orchestra limestone pavement and lower block of seats (Fig. 4b-c). High resolution topographic surveys carried out along several transects on features considered as a horizontal datum (i.e., flagstones and seat rows), show 50-to-60 cm of vertical net throw with downthrown side to the E (Fig. 7), including both discrete and distributed deformation.

Photos taken in 2009 during the archaeological excavation show that normal displacement affects Roman-age floorings as well as debris flow sediments covering the Theatre pavement (Fig. 5). The sediments are well-bedded for their entire exposure, except for a few meters wide zone, corresponding with the fault zone.

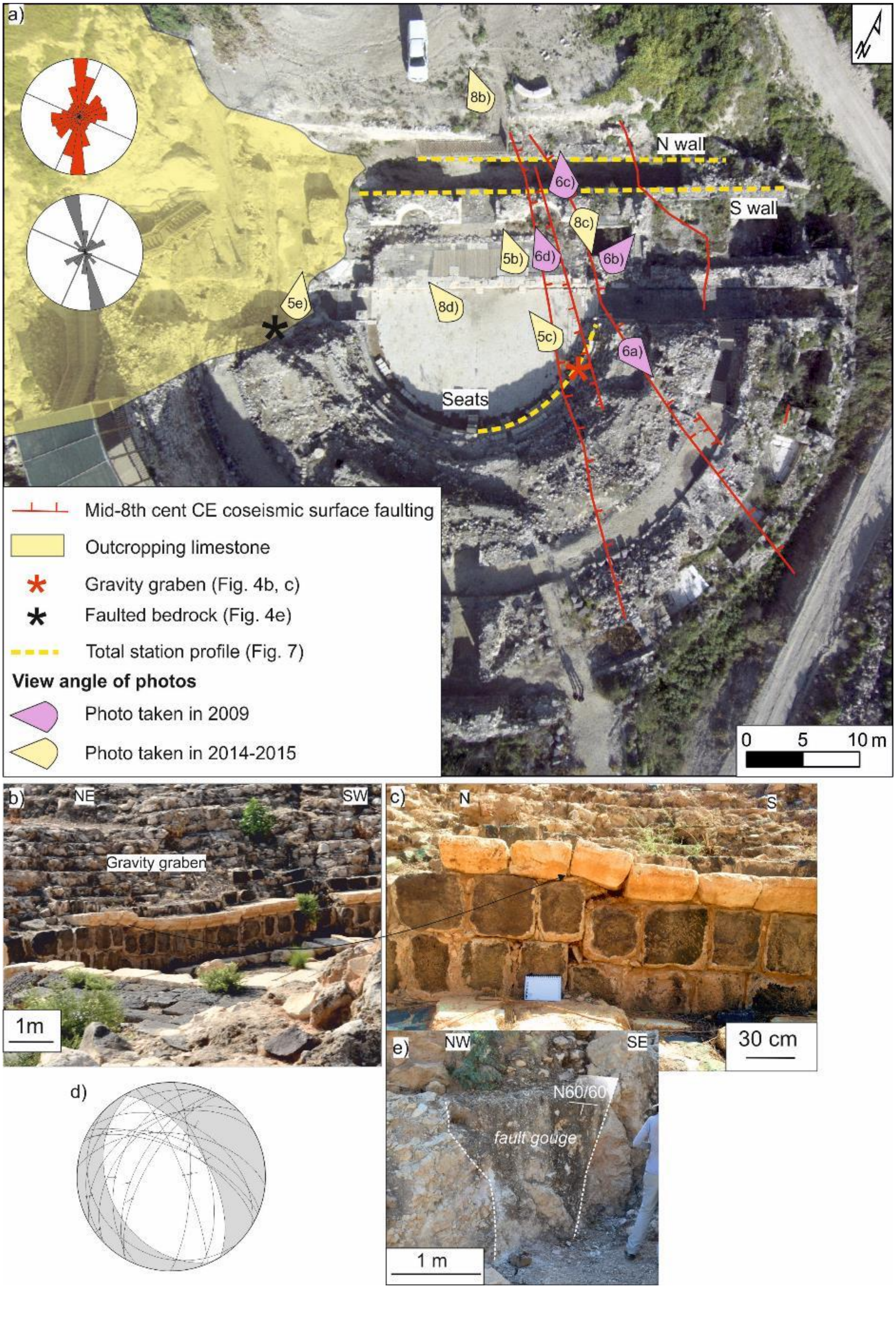
a)
8b)
N wall
6c)
S wall
8c)
5b)
6d)
6b)
5e)
8d)
5c)
6a)
Seats
Mid-8th cent CE coseismic surface faulting
Outcropping limestone
Gravity graben (Fig. 4b, c)
Faulted bedrock (Fig. 4e)
Total station profile (Fig. 7)
View angle of photos
Photo taken in 2009
Photo taken in 2014-2015
0 5 10 m
b)
NE
SW
Gravity graben
1m
c)
N
S
30 cm
d)
e)
NW
SE
N60/60
fault gouge
1 m

298

Figure 4. *Surface faulting at the Tiberias Theatre: a) map of ruptures across the Theatre, rose diagrams (bin size 15°) show fractures on archaeological relics from the whole site (red, n° 100) and on the orchestra floor (grey, n° 23); picture view angles (the figure number showing each picture is indicated) and trace of total station profiles are shown as well; b-c) details of the gravity graben displacing seat rows and walls; d) right dihedral best fit solution of fault slip inversion (15 fault planes in the limestone bedrock; Table S3); e) detail of the limestone normal fault gouge (site is shown in a).*

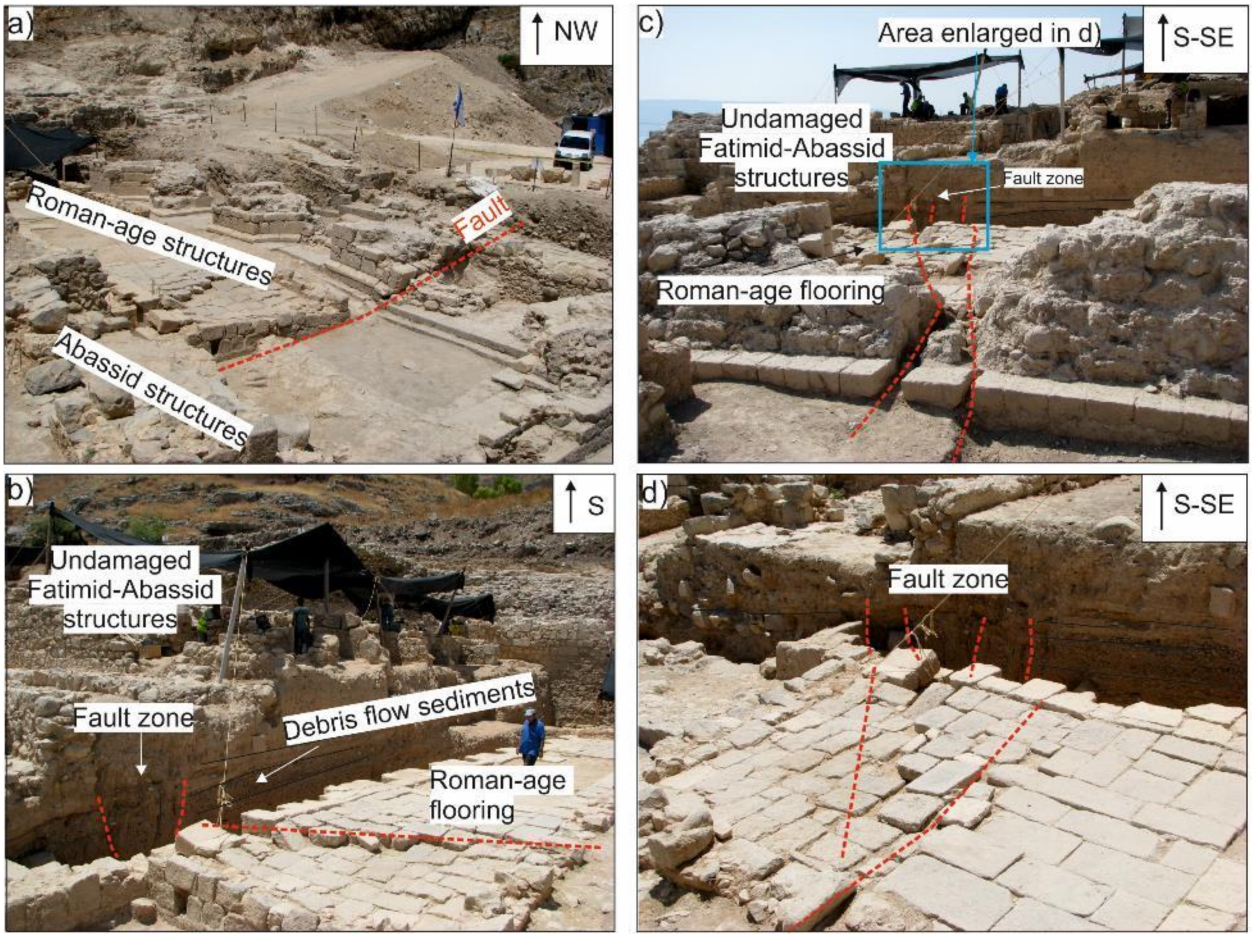

Figure 5. *Interpreted photographs taken during excavations at Tiberias Theatre in 2009 (photo courtesy of S. Marco). a) panoramic view on damaged Roman-age structures (fault trace is marked by red dashed line) overlaid by Fatimid-Abassid undamaged structures; b) damaged Roman Theatre flooring overlaid by faulted alluvial sediments (fault trace is marked by red dashed line) and undamaged Fatimid-Abassid structures; c) damaged Roman Theatre wall, overlaid by faulted alluvial sediments; d) detail of the damaged Roman flooring and the faulted alluvial sediments.*

The Southern Gate is built on a bedrock (Cretaceous limestone), which outcrops at the base of the wadi channel which runs in a general E-W direction within the site. Displacement at the Southern Gate is represented by warping of a Byzantine E-W wall, archaeologically dated at ca. 530 CE (Fig. 6b-c). A total station profile shows ca. 45 cm of total throw with downthrown side to the E (Fig. 7e). The measured displacement has a pure normal component with an amount of vertical displacement similar to that recorded at the Theatre.

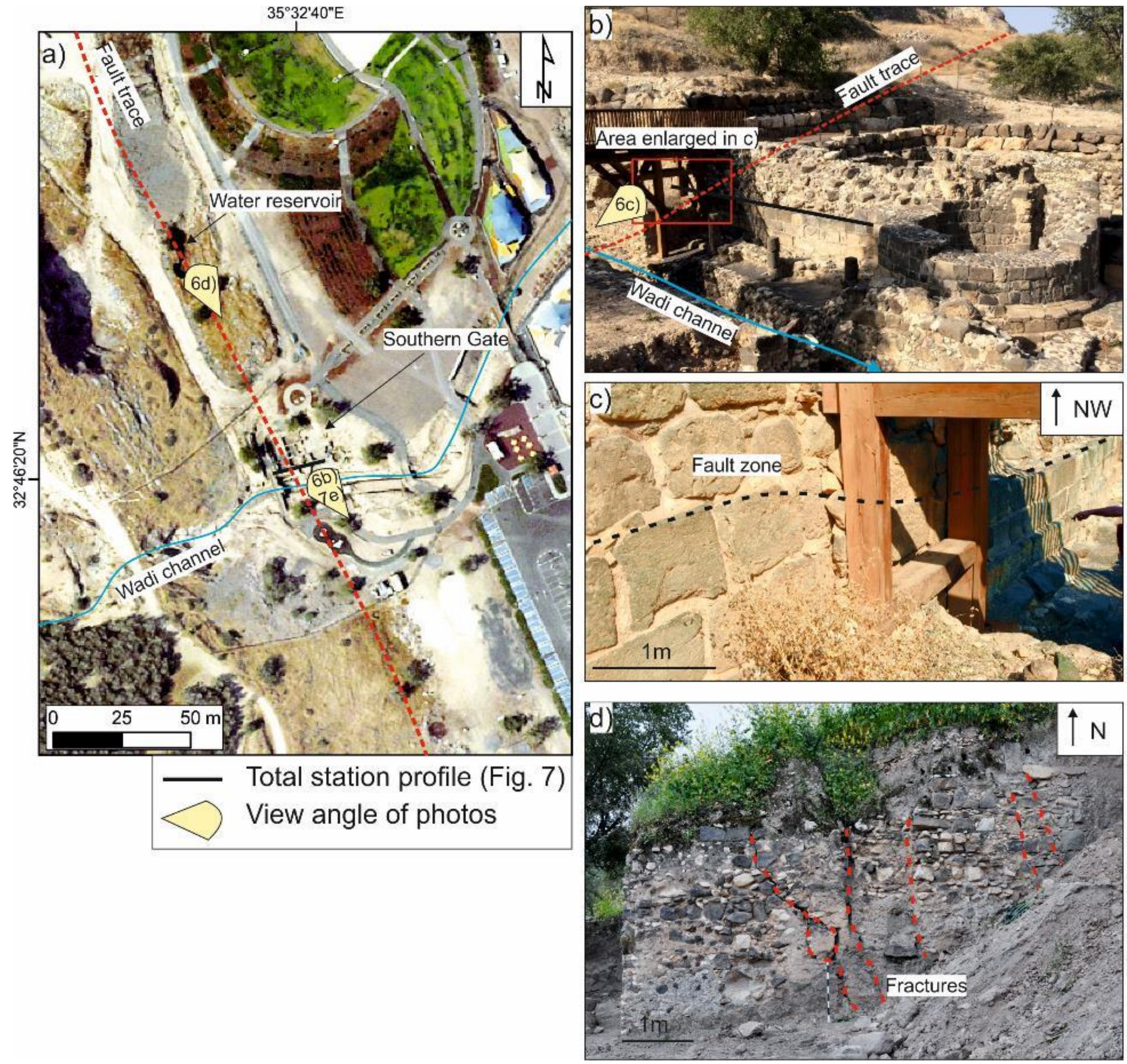

Figure 6*. a) Map of the Southern Gate and water reservoir sites, ca. 200 m S of the Theatre, along the JVWB Fault strike, with indication of picture view angles and trace of total station profile. Fault trace is marked by red dashed line; b) view of the Byzantine wall at the Southern Gate site; c) detail of the warped Byzantine wall. The wooded frame, holding the pedestrian bridge, is situated above the fault line. The dashed black line marks a down throw of an originally horizontal datum; d) set of fractures affecting an Umayyad water reservoir, located in between the Theatre and the Southern Gate.*

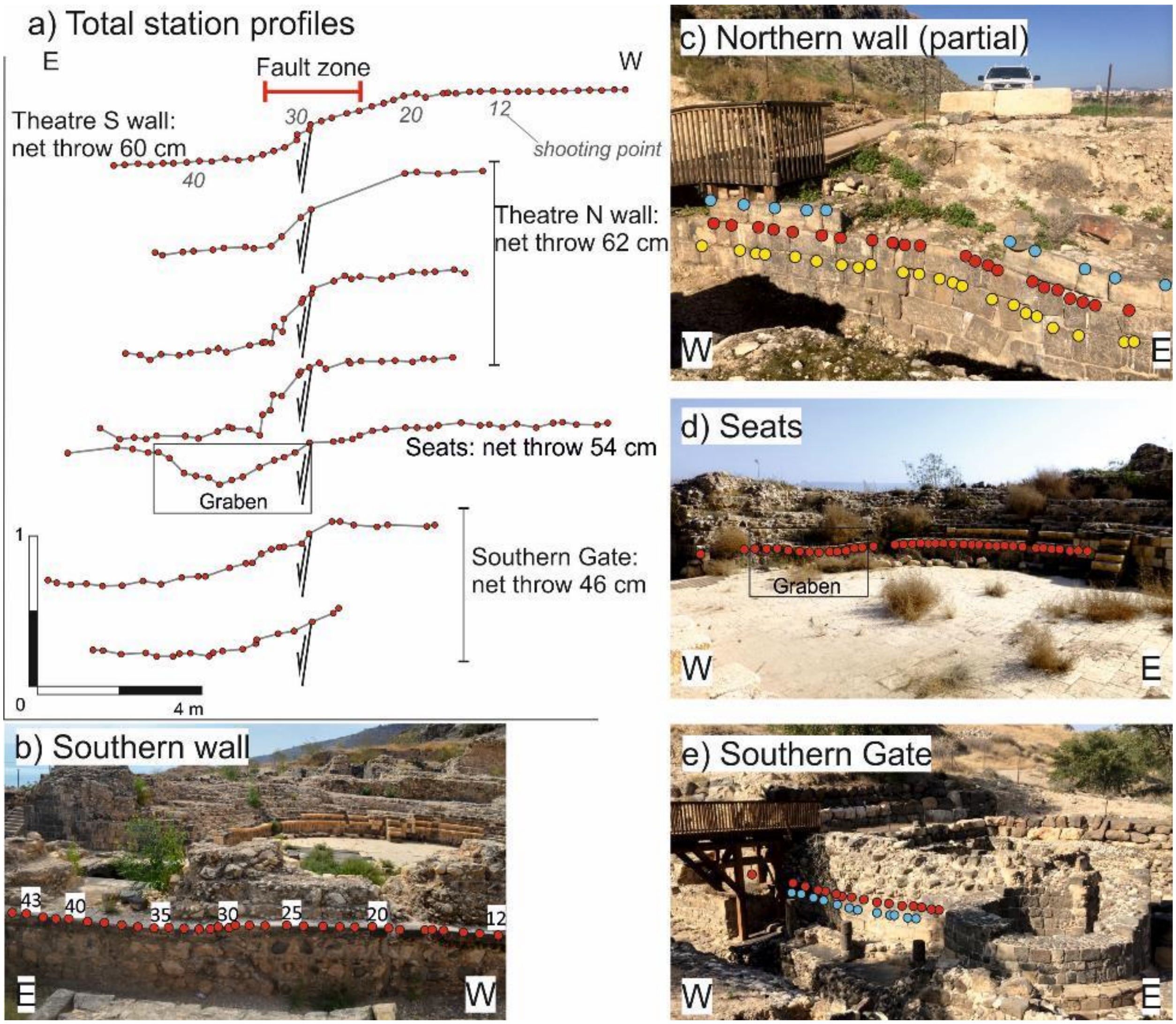

***Figure 7**. a) Topographic profiles obtained with a total station showing the vertical displacement across the studied fault at Tiberias Theatre and the Southern Gate. Each profile is plotted on a relative vertical scale with a vertical exaggeration of ca. 4x; b-e) photos of the measured points at Theatre (b-d) and Southern Gate (e), colored dots represent shooting points.*

4.1.2 Archaeological evidence for damage due to shaking

Beside the major damage described in section 4.1.1, the investigated sites show extensive strain features generated by transient shaking (Rodriguez-Pascua et al., 2011), such as fractures and cracks in masonry blocks and broken corners.

We measured dip and dip direction of 123 fractures (in masonry blocks) in the Theatre and 59 in the Southern Gate (Table S2). They are Mode I fractures (opening fractures), affecting walls and building stones. Generally, they break the entire stone height, albeit in some cases they affect a single corner of the building stone (see Fig. S2 for examples). The strike of the fractures has a modal value of 160° and 140° in the whole Theatre and the orchestra floor, respectively (see rose diagrams in Fig. 4a). These values are broadly consistent with the direction of the gravity graben found within the Theatre.

South of the Theatre, the last excavation phase during 2017 uncovered an Umayyad water reservoir. Damage is here represented by a series of steeply inclined fractures between masonry blocks, located in a ca. 1 m wide zone (Fig. 6d). The damage zone is situated along the line connecting the graben in the Theatre and the warped Byzantine wall at the Southern Gate, i.e. on the fault line.

4.1.3 *Terminus ante quem* for the damaging event: the Fatimid-Abassid quarter

The most recent building phase excavated at the Theatre site includes several buildings belonging to the Fatimid-Abassid period (Fig. 3a). Fig. 5 shows photos taken during excavations in 2009, when the Fatimid-Abassid quarter was not yet removed. In particular, Fig. 5b-d show that the damage is limited to the Roman-age flooring and to the debris flow sediments above it. The Fatimid-Abassid buildings, which lie immediately above the debris flow deposits, are never faulted nor deformed. This observation provides a tight *terminus ante quem* for the event that damaged the Theatre, i.e., not later than the 8^{th} – 11^{th} century CE.

Summary of the archaeoseismic observations reveals a ~300 m long segment of the JVWB (Theatre to Gate) that ruptured the surface during an earthquake that apparently took place at the 8^{th} century CE. Slip along the fault is normal, vertical throw is ~0.5 m.

4.2 The Jordan Valley Western Boundary fault: geomorphology and shallow subsurface

To trace the JVWB further N and S of the studied archeological sites, we acquired a series of seismic lines, dug an exploratory trench on the fault trace, interpreted available borehole logs and looked for geomorphological evidence of active tectonics along-strike of the JVWB through field surveys and LiDAR interpretation.

The Northern seismic line (Fig. 8), 500 m long, runs ~700 m N of the Tiberias Theatre. This high-resolution reflection line images to the SW a sequence characterized by a poorly resolved chaotic facies, possibly affected by edge effects, and ca. 3000 m/s Vp velocity; geological maps as well as surface outcrops allow to attribute this seismic facies to the Cretaceous limestones. A main high-angle normal fault segment, located in the westernmost part of the line, juxtaposes the limestones to Neogene-Quaternary deposits (Vp ca. 2200 m/s). More to the E (at ca. 300 m along-strike in Fig. 8), a second normal fault dissects the Neogene-Quaternary deposits and splays in several branches toward the surface, above ca. 200 mSec depth. A major sequence boundary at ca. 50 mSec marks the bottom of chaotic sediments downlapping in the uphill sector, that were interpreted as Late Pleistocene loose deposits (Vp < 1000 m/s). These latter can be attributed to different processes, including lacustrine, slope movement and man-made reworking. The E fault cut through this young sedimentary unit.

Line 253, a 250 m long reflection line, is located close to the Southern Gate (Fig. 9a). As was observed in the Northern line, Neogene-Quaternary deposits, locally showing onlap terminations, are cut by high-angle normal faults and overlaid by chaotic loose sediments. The westernmost fault revealed in this section corresponds with a subtle topographic scarp (Fig. 2b) identified on aerial photos and that can be faintly seen in the field. An exploratory trench 15 m long and 2.5 m deep was excavated across this scarp (Fig 2b). The trench revealed reworked archeological strata throughout its entire depth. We do not discuss in detail the trench because it gave inconclusive results: a cavity with human bones was found at the trench bottom, thus preventing further excavations. The oldest uncovered artifacts can be approximately dated at the

11th century CE. No evidence for faulting was observed in the trench section, in agreement with the archaeoseismic observations of the last earthquake along the JVWB in the 8th century CE.

Additional reflection line, 700 m long, is located 2.5 km S of the Theatre (Line 252; Fig. 2b, 9b), where a late Pleistocene landslide was previously interpreted as seismically triggered (Yagoda-Biran et al., 2010; Katz et al., 2010). Here, normal faults can be inferred, but the interpretation is not straightforward. At this site, we extract a 500-m long topographic profile from the LiDAR-derived DSM: the landslide toe is crossed by a 5.4-m high scarp, possibly fault-driven (Fig. S3).

Further constraints on the shallow subsurface are provided by stratigraphic logs of more than 30 boreholes (see Fig. 2b) located in the immediate closeness of the study area. We pinpoint the depth of stratigraphic or lithological boundaries and used this information to constrain the 3D geometry of the layers. The typical stratigraphic column comprises, from top to bottom, i) man-made infill, ii) loose deposits including clasts, clays and basalt fragments, iii) Pleistocene lacustrine marls and iv) bedrock. Boreholes in Fig. 2b are divided in two groups according to the depth of bedrock (i.e., thickness of loose deposits). It ranges from zero where bedrock is outcropping, to over 40 m depth. The whole coastal area and boreholes located at the outlet of wadi channels or on landslide deposits show more than 10 m of loose sediments, consistently with recent sedimentation processes. We use the few boreholes showing bedrock at depths shallower than 10 m as spatial constraints for the fault position.

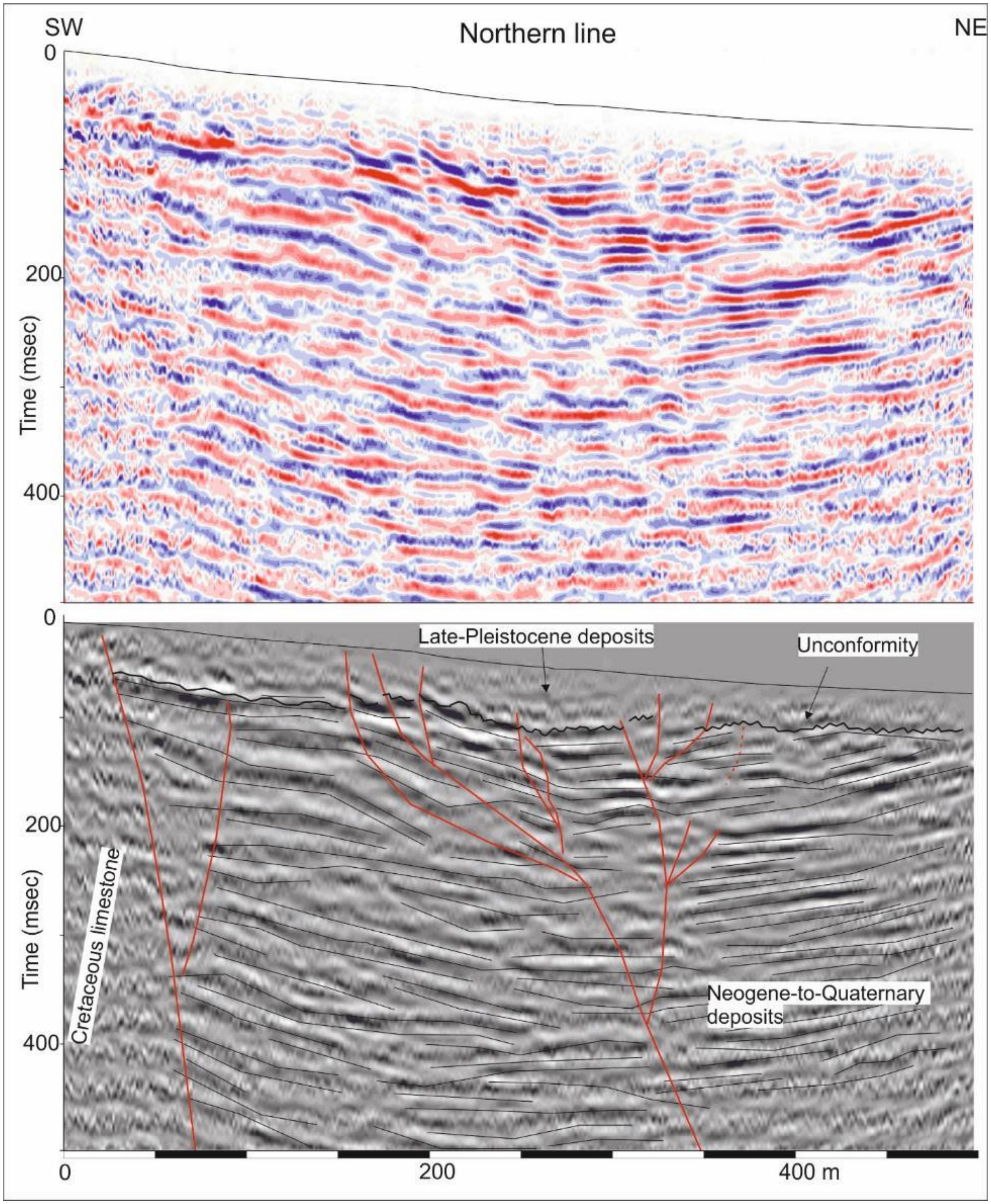

Figure 8. *Seismic line run N of Tiberias Theatre and relative interpretation; traces in Fig. 2a.*

412

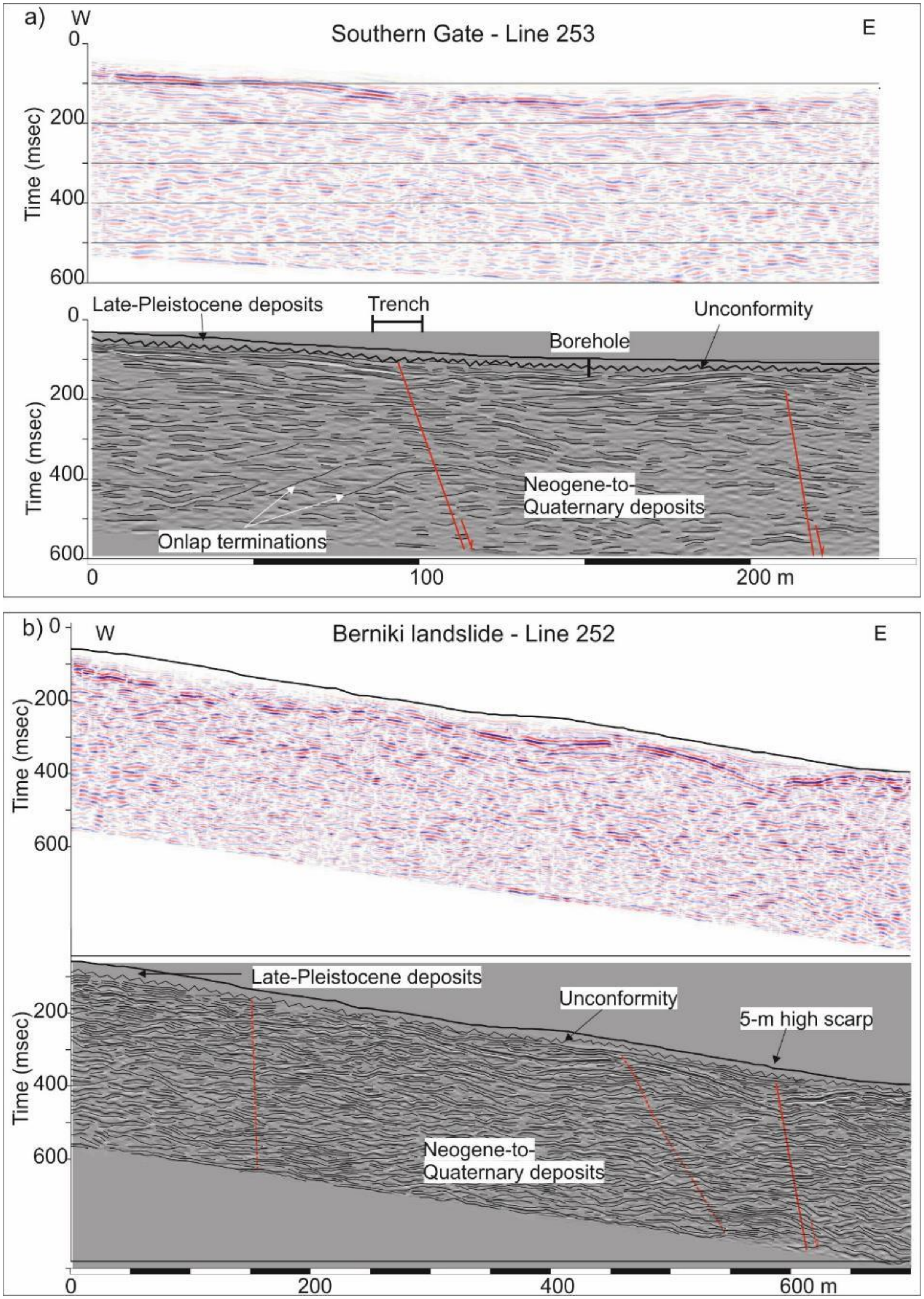

a)
W
Southern Gate - Line 253
E
Time (msec)
0
200
400
600
Late-Pleistocene deposits
Trench
Unconformity
Borehole
Neogene-to-
Quaternary deposits
Onlap terminations
0
100
200 m
b)
W
Berniki landslide - Line 252
E
Late-Pleistocene deposits
Unconformity
5-m high scarp
Neogene-to-
Quaternary deposits
400
600 m

Figure 9*. Seismic lines and relative interpretation; traces in Fig. 2a. a) Southern Gate. b) Berniki Beach landslide.*

5 Discussion and interpretations

5.1 What generated the damage observed at Tiberias?

Damage of archaeological sites can be due to a number of natural or man-made events. Ascribing that damage to a specific factor means to exclude other possible causes. In the case of Tiberias described in the present research, the following findings support surface rupture as the causative mechanism:

i) The investigated sites are built on a contact between limestones and thin (few meters) alluvial deposits; the presence of shallow limestone bedrock beneath the hangingwall alluvial deposits is also confirmed by boreholes. Bedrock outcrops inside the Theatre and at the bottom of the wadi channel at the Southern Gate.

ii) All damaged sites are aligned along a lineament in a N140 direction, which is consistent with the structural framework of the study area.

iii) All our observations document a pure dip-slip normal faulting.

iv) The gravity-graben inside the Theatre is a feature consistent with coseismic, near-fault deformation (e.g., Slemmons, 1957; Rodriguez-Pascua et al., 2011) and possibly due to the steepening of the fault plane approaching the surface.

v) Damage is consistently found in Roman levels and in the debris flow sediments uncovered in the Theatre, but the Abassid levels were not faulted nor deformed. Archaeological stratigraphy provides tight chronological constraints, based on architectural style, building techniques and materials of the findings and structures.

The lines of reasoning listed above point toward an earthquake-related damage, and more specifically to surface faulting. The damaging event is constrained to later than 530 CE and younger than the Abassid caliphate (750-1258 CE). Among the historical records of strong earthquakes that hit the area and might have been accompanied by surface faulting, the only one fitting with this chronological interval is the mid-8th century CE seismicity (Fig. 3).

The presence of a thick cover of man-made deposits, intensely reworking and eroding the natural landscape, partly justifies the difficulty in here recognizing tectonic landforms. The lack of deformation since medieval times at the investigated sites suggests the absence of soil movements due to local differential settlement, compaction, landsliding, slope processes or aseismic creep in the closeness of the faulted archaeological sites. In fact, several strong seismic events occurred at Tiberias after the 8th century CE sequence, such as the 1759 and 1837 events (Ambraseys & Barazangi, 1989; Ambraseys, 1997). Severe shaking during these seismic events did not reactivate the mapped fault ruptures at the Theatre and Southern Gate. This rules out a purely geotechnical and/or gravitational control on the observed fault ruptures. This is further confirmed by the exploratory trench that we excavated along-strike of the fault observed at the Theatre and Southern Gate. The unearthed sediments do not show any sign of deformation due to tectonic processes and/or slope movements down to the 11th century CE.

Fig. 3b shows the sites where surface faulting has been related to the mid-8th century CE seismicity (see also Section 2.3). Ruptures may have been caused by a single earthquake or by a sequence of events, a topic that we address in Section 5.3.

5.2 Structural setting and fault displacement hazard at Tiberias

The reconstruction of the stratigraphic and structural setting of the shallow subsurface (Fig. 10) shows faults reaching the surface; they were constrained by direct observation at the archaeological sites (Fig. 10a-b) or presence of the hotsprings (Fig. 10c). Other faults were imaged through the seismic lines and borehole correlation.

Our data suggest the presence of a fault zone some tens of meters wide, rather than a single fault. At the Theatre (Fig. 10a) and at the Northern seismic line (Fig. 9), we observe to the W a fault strand at the contact between Cretaceous limestone and the Neogene-Quaternary deposits; to the E, a second fault strand lies within the Neogene-Quaternary deposits. At the Theatre, the fault gouge in Cretaceous limestones (Fig. 4e) show no signs of historical displacements, whereas the archaeological structures are faulted more to the E (Fig. 4a). This may suggest a basinward migration of the active fault strand, consistently with previous observations at other sites along the DSF (Marco & Klinger, 2014). At the Southern Gate the fault lies within Cretaceous limestones, as deduced from archaeoseismological observations and core drillings (Fig. 10b).

The heterogeneous lithological and stratigraphic setting has implications for fault displacement hazard assessment: the different properties of bedrock and loose sediments affect the fault pattern and expression at the surface, including amount of displacement (Bray et al., 1994). The complex interplay between coseismic surface faulting and the lithological setting has been pointed out by several recent investigations (e.g., Teran et al., 2015; Gold et al., 2015; Hornsby et al., 2019; Livio et al., 2020). Such heterogeneous expressions of coseismic surface faulting should be incorporated into the development of building codes and regulations specifically targeted at fault displacement hazard assessment (Youngs et al., 2003; Petersen et al., 2011; ANSI/ANS-2.30, 2015).

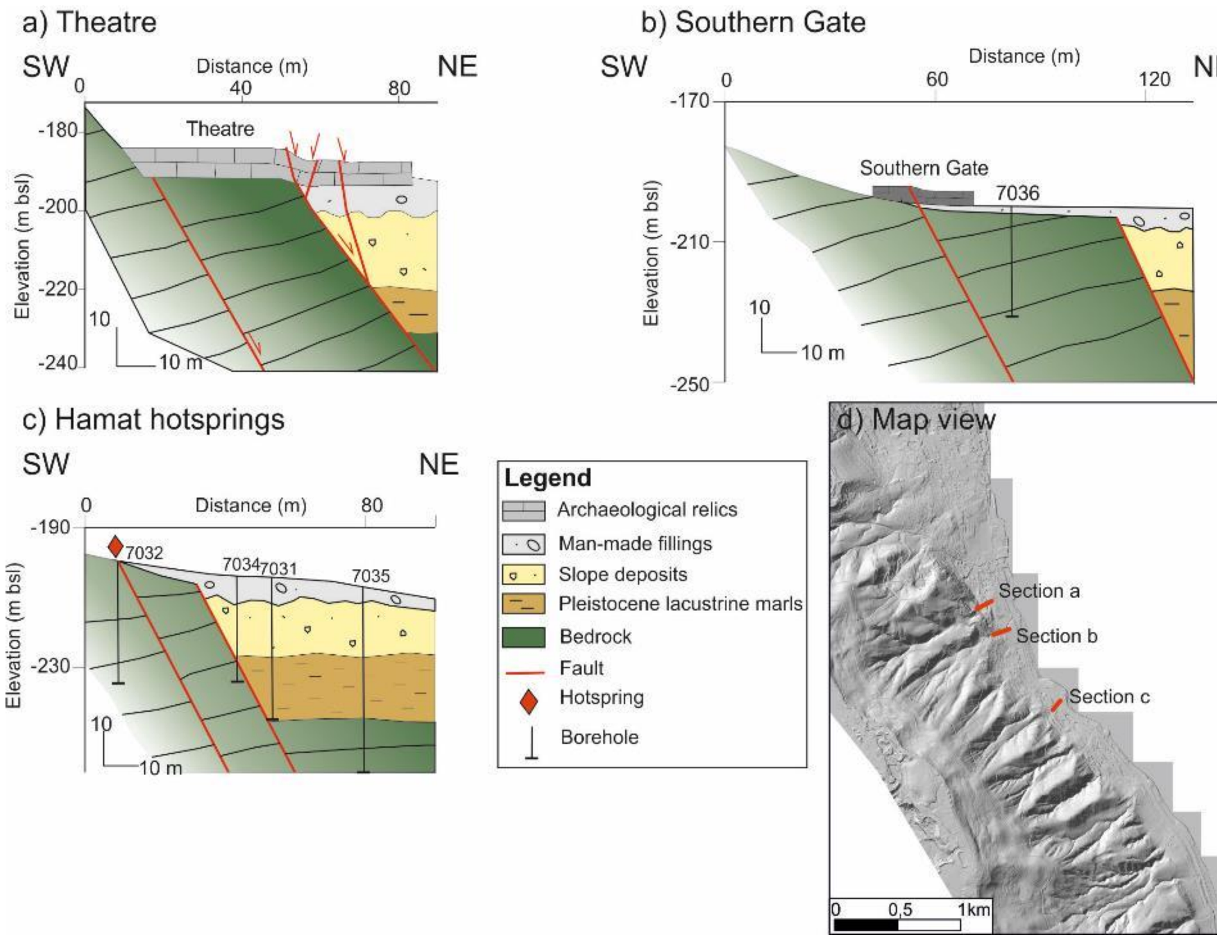

Figure 10. *Schematic sketches of the shallow subsurface at three key positions: a) Theatre; b) Southern Gate; c) Hamat hotsprings. Information on geology is derived from the Israeli geological map (Sneh, 2008), published scientific literature (e.g., Hurwitz et al., 2002) and local reports (e.g., Zaslavsky, 2009). Boreholes logs are from GSI archive; d) section traces.*

5.3 Rupture scenarios

For better constraining the seismic hazard for the area, we consider three different rupture scenarios and calculate expected magnitude from known fault length and area adopting published scaling relations (Wells & Coppersmith, 1994; Hanks & Bakun, 2008; Wesnousky, 2008; Stirling et al., 2013). Two scenarios include the rupture of a single normal fault source, i.e. the Jordan Valley Western Boundary Fault (JVWB, scenario n° 1), assuming it is continuous at the subsurface as a worst-case scenario, or the Jordan Valley Fault (JVF, scenario n° 2). The third scenario accounts for the simultaneous rupture of the JVWB and JVF. Inversion of geodetic measurements as well as moderate seismicity cutoff depth indicate a locking depth of 10-15 km (Sadeh et al., 2012; Hamiel et al., 2016), close to the upper-lower crust transition (ten Brink et al., 2006), even if some works claim a deeper transition (ca. 28 km according to Garfunkel et al., 2014). The JVF and JVWB are linked above or close to the locking depth, and thus can rupture separately or together (single- or multi-fault rupture scenario *sensu* Lettis & Hanson, 1991).

For calculating the expected magnitudes, we assumed the following parameters for the faults:

- Scenario n° 1 – JVWB: normal faulting, length 45 km (Tiberias to Tel Rehov and Tel Teomim);
- Scenario n° 2 – JVF: strike-slip faulting, length 125 km (from Beteiha to Jericho), width 12.5 km;
- Scenario n° 3 – JVWB and JVF: normal and strike-slip faulting, length 170 km (sum of scenario 1 and 2), width 12.5 km.

In the selection of the most appropriate scaling relation, we rely on the work by Stirling et al. (2013), who compiled published scaling relationships and categorized them according to tectonic regime and style of faulting. They also assign a quality score based on the quality and quantity of the regression dataset. Following these guidelines, we select the subclass A2 which represents slow plate boundary faults (< 10 mm/yr) as the one most suitable to rates measured along the DSF. The slip rates along the DSF are indeed constrained to 4-5 mm/yr from geological and GPS data (Garfunkel et al., 2014).

For the scenario n° 1 (normal faulting), we select the scaling relation published by Wesnousky (2008), which has a quality score 1 (i.e., best available) according to Stirling et al. (2013). Moment magnitude Mw is computed from surface rupture length L as:

$$Mw = 6.12 + 0.47 \log L$$

Resulting in an estimated Mw = 6.9 for the JVWB rupture.

For the scenarios n° 2 and 3, we select the relation by Hanks and Bakun (2008), which has a quality score 1 (i.e., best available) according to Stirling et al. (2013). For areas larger than 537 square kilometers, moment magnitude Mw is computed from fault area A as:

$$Mw = 4/3 \log A + (3.07 \pm 0.04)$$

Scenario n° 2 results in an estimated magnitude of 7.3, whereas scenario n° 3 results in Mw = 7.6.

When exploring different parametrizations (i.e., fault rupture length, fault width, adopted scaling relations), we find estimated magnitudes consistent with the preferred ones (i.e., differences of up to 0.1).

Scenario n° 3 implies the coexistence of dip-slip and lateral motions. Such setting can be explained by strain partitioning, a phenomenon already documented elsewhere along the DSF (Ben-Avraham and Zoback, 1992; Sagy et al., 2003; Makovsky et al., 2008; Weinberger et al., 2009) and worldwide (e.g., Lettis & Hanson, 1991; Walker et al., 2005).

Summarizing, we obtain a maximal Mw 6.9 for the JVWB rupture and a Mw 7.3 for the JVF. The multi-fault scenario results in a Mw 7.6 earthquake. Our magnitude estimates are consistent with those suggested in the literature (i.e., Ms 7.0 – 7.5; Marco et al., 2003; Hamiel et al., 2009; Zohar et al., 2016), but we underline that our calculations represent worst-case scenarios, which imply the rupture of the entire fault. Complete fault ruptures may be obstructed by structural thresholds; we maintain that partial fault ruptures may occur as well, resulting in smaller magnitudes. The simultaneous rupture of JVWB and JVF for their entire lengths

(Scenario n° 3) is considered unlikely, but such occurrence should not be discarded in seismic hazard evaluations.

Other events may have occurred in the mid-8th century CE more to the N (Yammouneh and/or Missyaf Faults) or S of the Dead Sea, but their evaluation is beyond the scope of the present paper.

The occurrence of multiple shocks in a close time interval is a common pattern in the DSF region, as clearly documented in the historical record (e.g., Karcz, 2004; Ambraseys, 2005, 2009) and by geological studies (Agnon, 2014; Marco and Klinger, 2014; Lefevre et al., 2018). The present study documents an additional fault with evidence of surface ruptures within a region with already known major active faults. This finding, coupled with earthquake clustering, will help to better depict the seismic landscape (Michetti et al., 2005) in the Sea of Galilee region.

6 Conclusions

The geometry, kinematics and activity of the faults crossing the town of Tiberias, studied through an integrated structural, archaeoseismological and geophysical approach revealed that this segment was activated in the mid-8th century CE.

We propose that normal dip-slip motion on the W side of the Sea of Galilee can coexist with strike-slip motion in the E side, in a strain-partitioned model. Based on the results of this study, we suggest that multi-fault rupture may be more frequent than the occurrence of single-fault ruptures in the Sea of Galilee region. This must be considered in any seismic hazard evaluation for this area. The absence of instrumental measurements of strong (Mw greater than 6.0) earthquakes with normal fault focal mechanism should not be construed as evidence that similar events will never occur along this section of the Dead Sea Fault.

The recent earthquake swarms that affected the Sea of Galilee region remind that a re-evaluation of the seismic risk is overdue. Our research provides useful inputs for developing updated building codes in the Tiberias area: measures to reduce exposure and the overall seismic risk (e.g., avoidance zones, setback distances) must rely on the unequivocal definition of active fault traces and their characterization. The 2018 swarm shows normal focal mechanisms and thus supports our claim that seismic source characterization in the Sea of Galilee, and along the DSF, must consider strain partitioning and fault interaction. We argue that the renewed attention of the public opinion, driven by the recent seismicity, can be an incentive to act on mitigation and preparedness measures.

Acknowledgments

We wish to thank Tiberias Municipality, the Israel Antiquity Authority, the Geophysical Institute of Israel, Y. Nahmias (GSI), E. Hassul and Y. Darvasi (Neev Center for Geoinformatics at the Hebrew University). We are grateful to Shmulik Marco for fruitful discussions and for kindly handing us the pictures of the Theatre excavations in 2009; to Amotz Agnon for helpful conversation on the seismic landscape of the Dead Sea Rift. Fondazione Banca del Monte di Lombardia fellowship allowed a 6-months stay of MFF at GSI. The work was supported by the

Israeli National Steering Committee for Earthquake Preparedness. Historical seismicity is from http://seis.gii.co.il/en/earthquake/searchEQSRslt.php, the reports on archaeological excavations are from http://www.hadashot-esi.org.il/default_eng.aspx (last accessed February 2020). Other data are available from the listed references.

References

Agnon, A., (2014). Pre-Instrumental Earthquakes Along the Dead Sea Rift. In Dead Sea Transform Fault System: Reviews, 207-261.

Alfonsi, L., Cinti, F.R., & Ventura, G. (2013). The Kinematics of the 1033 AD Earthquake Revealed by the Damage at Hisham Palace (Jordan Valley, Dead Sea Transform Zone). Seism. Res. Lett., 84(6), 997-1003.

Allmendinger, R.W., Marrett, R.A., & Cladouhos, T.T. (2001). FaultKinWin: a program for analyzing fault slip data for Windows™ computers. http://www.geo.cornell.edu/geology/faculty/RWA/programs/

Ambraseys, N. (1997). The earthquake of 1 January 1837 in Southern Lebanon and Northern Israel. Ann. Geofis. XL (4), 923–935.

Ambraseys, N. N. (2005). The seismic activity in Syria and Palestine during the middle of the 8th century; an amalgamation of historical earthquakes. J of Seism, 9(1), 115-125.

Ambraseys, N. (2009). Earthquakes in the Mediterranean and Middle East: a multidisciplinary study of seismicity up to 1900: Cambridge University Press.

Ambraseys, N., & Barazangi, M. (1989). The 1759 Earthquake in the Bekaa valley: implications for earthquake hazard assessment in Eastern Mediterranean region. J. Geophys. Res. 94, 4007–4013.

ANSI/ANS-2.30 (2015). Criteria for assessing tectonic surface fault rupture and deformation at nuclear facilities, Published by the American Nuclear Society.

Atrash, W. (2010). Tiberias, the Roman Theater. http://www.hadashot-esi.org.il/report_detail_eng.aspx?id=1381&mag_id=117

Ben-Avraham, Z., & Zoback, M. (1992). Transform-normal extension and asymmetric basins: an alternative to pull-apart models. Geology, 20, 423-426.

Bogoch, R., & Sneh, A. (2008). Geological map of Israel, 1:50,000, Sheet 4-I Arbel. GSI, Jerusalem.

Bozorgnia, Y., & Bertero, V. V. (2004). Earthquake engineering: from engineering seismology to performance-based engineering. CRC press.

Bray, J. D., Seed, R. B., Cluff, L. S., & Seed, H. B. (1994). Earthquake fault rupture propagation through soil. Journal of Geotechnical Engineering, 120(3), 543-561.

Dalali-Amos, E. (2016). Excavations at Tiberias, Final report, Hadashot Arkheologiyot, 128 http://hadashot-esi.org.il/report_detail_eng.aspx?id=25056&mag_id=124

Daëron, M., Klinger, Y., Tapponnier, P., Elias, A., Jacques, E., & Sursock, A. (2007). 12,000-year-long record of 10 to 13 paleoearthquakes on the Yammouneh fault, Levant fault system, Lebanon. Bulletin of the Seismological Society of America, 97(3), 749-771.

Eppelbaum, L.V., Ben-Avraham, Z., & Katz, Y. (2007). Structure of the Sea of Galilee and Kinarot Valley derived from combined geological geophysical analysis. First break, 25(1), 43-50.

Ferry, M., Meghraoui, M., Abou Karaki, N., Al-Taj, M., Amoush, H., Al-Dhaisat, S., & Barjous, M. (2007). A 48-kyr-long slip rate history for the Jordan Valley segment of the Dead Sea fault. EPSL 260, 394–406.

Garfunkel, Z. (1981). Internal structure of the Dead Sea leaky transform (rift) in relation to plate kinematics. Tectonophysics 80, 81–108.

Garfunkel, Z., Ben-Avraham, Z., & Kagan, E. (Eds.) (2014). Dead Sea transform fault system: reviews. Vol. 6, Springer.

Gold, P. O., Oskin, M. E., Elliott, A. J., Hinojosa-Corona, A., Taylor, M. H., Kreylos, O., & Cowgill, E. (2013). Coseismic slip variation assessed from terrestrial LiDAR scans of the El Mayor–Cucapah surface rupture. Earth and Planetary Science Letters, 366, 151-162.

Guidoboni, E., Ferrari, G., Mariotti, D., Comastri, A., Tarabusi, G., & Valensise, G. (2007). Catalogue of Strong Earthquakes in Italy (461 BC-1997) and Mediterranean Area (760 BC-1500).

Hamiel, Y., Amit, R., Begin, Z. B., Marco, S., Katz, O., Salamon, A., Zilberman, E., & Porat, N. (2009). The seismicity along the Dead Sea Fault during the last 60,000 years. Bulletin of the Seismological Society of America, 99(3), 2020-2026.

Hamiel, Y., Piatibratova, O., & Mizrahi, Y. (2016). Creep along the northern Jordan Valley section of the Dead Sea Fault. Geophys Res Lett, 43.

Hanks, T. C., & Bakun, W. H. (2008). M − log A observations of recent large earthquakes. Bull. Seismol. Soc. Am., 98(1), 490–494.

Hartal, M., Dalali-Amos. E., & Hilman, A. (2010). Preliminary report on the excavations at Tiberias. http://hadashot-esi.org.il/report_detail_eng.aspx?id=1574&mag_id=117

Hazan, N., Stein, M., Agnon, A., Marco, S., Nadel, D., Negendank, F.W., et al. (2005). The late Quaternary limnological history of Lake Kinneret (Sea of Galilee). Israel Quat Res 63, 60–77.

Hirschfeld, Y., & Meir, E. (2004). Tiberias, Hadashot Arkheologiyot, 118, http://www.hadashot-esi.org.il/report_detail_eng.aspx?id=337&mag_id=111

Hirschfeld, Y., & Gutfeld, O. (2008). Tiberias. Excavations in the House of the Bronzes. Final Report, Volume I. Qedem Monographs of the Institute of Archaeology.

Hornsby, K. T., Streig, A. R., Bennett, S. E., Chang, J. C., & Mahan, S. (2019). Neotectonic and Paleoseismic Analysis of the Northwest Extent of Holocene Surface Deformation along the Meers Fault, Oklahoma. Bulletin of the Seismological Society of America.

Hurwitz, S., Garfunkel, Z., Ben-Gai, Y., Reznikov, M., Rotstein, Y., & Gvirtzman, H. (2002). The tectonic framework of a complex pull-apart basin: seismic reflection observations in the Sea of Galilee, Dead Sea transform. Tectonophysics, 359(3), 289-306.

Ilani, S., Minster, T., Kronfeld, J., & Even, O. (2006). The source of anomalous radioactivity in the springs bordering the Sea of Galilee. Israel, J of env radioactivity, 85(1), 137-146.

Karcz, I. (2004). Implications of some early Jewish sources for estimates of earthquake hazard in the Holy Land. Ann of Geoph, 47(2-3).

Katz, O., Amit, R., Yagoda-Biran, G., Hatzor, Y., Porat, N., & Medvedev, B. (2010). Quaternary earthquakes and landslides in the Sea of Galilee area, the Dead Sea Transform; paleoseismic analysis and evaluation of current hazard. Isr J Earth Sci, 58: 275-294.

Lefevre, M., Klinger, Y., Al-Qaryouti, M., Le Béon, M., &Moumani, K. (2018). Slip deficit and temporal clustering along the Dead Sea fault from paleoseismological investigations. Scientific reports, 8(1), p.4511.

Lettis, W.R., & Hanson, K.L. (1991). Crustal strain partitioning: Implications for seismic-hazard assessment in western California. Geology, 19(6), 559-562.

Livio, F. A., Ferrario, M. F., Frigerio, C., Zerboni, A., & Michetti, A. M. (2020). Variable fault tip propagation rates affected by near-surface lithology and implications for fault displacement hazard assessment. Journal of Structural Geology, 130, 103914.

Makovsky, Y., Wunch, A., Ariely, R., Shaked, Y., Rivlin, A., Shemesh, A., Avraham, Z.B., & Agnon, A. (2008). Quaternary transform kinematics constrained by sequence stratigraphy and submerged coastline features: The Gulf of Aqaba. Earth and Planetary Science Letters, 271(1-4), 109-122.

Marco, S., & Klinger, Y. (2014). Review of On-Fault Palaeoseismic Studies Along the Dead Sea Fault. In Dead Sea Transform Fault System: Reviews, 183-205.

Marco, S., Hartal, M., Hazan, N., Lev, L., & Stein, M. (2003). Archaeology, history, and geology of the A.D. 749 earthquake, Dead Sea Transform. Geology, 31 (8) 665-668.

Marco, S., Rockwell, T.K., Heimann, A., Frieslander, U., & Agnon, A. (2005). Late Holocene activity of the Dead Sea Transform revealed in 3D palaeoseismic trenches on the Jordan Gorge segment. Earth and Planetary Science Letters 234 (2005) 189– 205.

Marrett, R., & Allmendinger, R.W. (1990). Kinematic analysis of fault-slip data. Journal of Structural Geology 12(8), 973–986.

Medvedev, B. (2008). Faults mapping in Berniki area, Western Sea of Galilee, The Geophysical Institute of Israel, report: 645/319/08 (in Hebrew). http://mapi.gov.il/earthquake/documents/j.pdf

Meghraoui, M., Gomez, F., Sbeinati, R., Van der Woerd, J., Mouty, M., Darkal, A. N., et al. (2003). Evidence for 830 years of seismic quiescence from palaeoseismology, archaeoseismology and historical seismicity along the Dead Sea fault in Syria. Earth and Planetary Science Letters, 210(1-2), 35-52.

Michetti, A. M., Audemard F. A., & Marco, S. (2005). Future trends in paleoseismology: Integrated study of the seismic landscape as a vital tool in seismic hazard analyses. Tectonophysics, 408(1-4), 3-21.

Onn, A., & Weksler-Bdolah, S. (2016). Tiberias, Gane Hammat, Hadashot Arkheologiyot 128 http://www.hadashot-esi.org.il/Report_Detail_Eng.aspx?id=25097

Petersen, M. D., Dawson, T. E., Chen, R., Cao, T., Wills, C. J., Schwartz, D. P., & Frankel, A. D. (2011). Fault displacement hazard for strike-slip faults. Bulletin of the Seismological Society of America, 101(2), 805–825.

Reches, Z., & Hoexter, D.F. (1981). Holocene seismic and tectonic activity in the Dead Sea area. Tectonophysics 80:235–254.

Rodriguez-Pascua, M. A., Pérez-López, R., Giner-Robles, J.L., Silva, P.G., Garduño-Monroy, V.H., & Reicherter, K. (2011). A comprehensive classification of Earthquake Archaeological Effects (EAE) in archaeoseismology: Application to ancient remains of Roman and Mesoamerican cultures. Quat Int 242(1), 20-30.

Rotstein, Y., Bartov, Y., & Frieslander, U. (1992). Evidence for local shifting of the main fault and changes in the structural setting, Kinarot basin, Dead Sea transform. Geology, 20(3), 251-254.

Sadeh, M., Hamiel, Y., Ziv, A., Bock, Y., Fang, P., & Wdowinski, S. (2012). Crustal deformation along the Dead Sea Transform and the Carmel Fault inferred from 12 years of GPS measurements. Journal of Geophysical Research, 117, 1-14.

Sagy, A., Reches, Z.E., & Agnon, A. (2003). Hierarchic three-dimensional structure and slip partitioning in the western Dead Sea pull-apart. Tectonics, 22(1).

Sagy, A., Sneh, A., Rosensaft, M., & Bartov, Y. (2016). Map of active faults and potentially active faults for the Israel Standard 413 “design provisions for earthquakes resistance of structures”, Update 2016. http://www.gsi.gov.il/_uploads/ftp/Active_Faults_maps/2016_map_English.pdf

Slemmons, D. B. (1957). Geological effects of the Dixie Valley – Fairview Peak, Nevada, earthquakes of December 16, 1954. Bulletin of the Seismological Society of America, 47(4), 353-375.

Sharon, M., Sagy, A., Kurzon, I., Marco, S., Ben-Avraham, Z., & Rosensaft, M. (2018). Quaternary fault map of Israel. Jerusalem, 2018 http://www.gsi.gov.il/_uploads/ftp/GeologicalMap/Quaternary_fault_Map_Israel.pdf

Sharon, M., Sagy, A., Kurzon, I., Marco, S., & Rosensaft M. (2020). Assessment of seismic sources and capable faults through hierarchic tectonic criteria: implications for seismic hazard in the Levant. Natural Hazards and Earth System Sciences, 20(1), 125-148, https://doi.org/10.5194/nhess-20-125-2020.

Sneh, A. (2008). Geological map of Israel, 1:50,000, Sheet 4-II Teverya: GSI, Jerusalem. http://www.gsi.gov.il/eng/?CategoryID=253&ArticleID=763

Sneh, A., & Weinberger, R. (2014). Major geological structures of Israel and environs, scale 1:500.000, Geological Survey of Israel. http://www.gsi.gov.il/eng/?CategoryID=298&ArticleID=751

Stirling, M., Goded, T., Berryman, K., & Litchfield, N. (2013). Selection of Earthquake Scaling Relationships for Seismic-Hazard Analysis. Bull. Seismol. Soc. Am., 103(6), 1-19.

Ten Brink, U., Rybakov, M., Al Zoubi, A.S., Hassouneh, M., Frieslander, U., Batayneh, A.T., et al. (1999). Anatomy of the Dead Sea transform: Does it reflect continuous changes in plate motion?. Geology, 27(10), 887-890.

Ten Brink, U., Al-Zoubi, A., Flores, C.H., Rotstein, Y., Qabbani, I., Harder, S.H. & Keller, G.R., (2006). Seismic imaging of deep low-velocity zone beneath the Dead Sea basin and transform fault: Implications for strain localization and crustal rigidity. Geophysical Research Letters, 33(24).

Teran, O. J., Fletcher, J. M., Oskin, M. E., Rockwell, T. K., Hudnut, K. W., Spelz, R. M., Akciz, S. O., Hernandez-Flores, A. P., & Morelan, A. E. (2015). Geologic and structural controls on rupture zone fabric: A field-based study of the 2010 Mw 7.2 El Mayor–Cucapah earthquake surface rupture. Geosphere, 11(3), 899–920. https://doi.org/10.1130/GES01078.1

Tsafrir, Y., & Foerster, G. (1992). The dating of the “Earthquake of the Sabbatical year” of 749 CE in Palestine. Bull of the School of Oriental and African Studies, Univ of London, 55(2), 231-235.

Walker, J. D., Kirby, E., & Andrew, J.E. (2005). Strain transfer and partitioning between the Panamint Valley, Searles Valley, and Ash Hill fault zones, California. Geosphere, 1(3), 111-118.

Wechsler, N., Rockwell, T.K., & Klinger, Y. (2018). Variable slip-rate and slip-per-event on a plate boundary fault: The Dead Sea fault in northern Israel. Tectonophysics, 722, 210-226.

Weinberger, R., Gross, M. R., & Sneh, A. (2009). Evolving deformation along a transform plate boundary: example from the Dead Sea Fault in northern Israel. Tectonics, 28(5).

Wells, D. L., & Coppersmith, K. J. (1994). New empirical relationships among magnitude, rupture length, rupture width, rupture area, and surface displacement. Bulletin of the seismological Society of America, 84(4), 974-1002.

Wesnousky, S.G. (2008). Displacement and geometrical characteristics of earthquake surface ruptures: Issues and implications for seismic hazard analysis and the process of earthquake rupture. Bull. Seismol. Soc. Am., 98(4), 1609–1632.

Wetzler, N., Shalev, E., Göbel, T., Amelung, F., Kurzon, I., Lyakhovsky, V., & Brodsky, E. E. (2019). Earthquake swarms triggered by groundwater extraction near the Dead Sea Fault. Geophysical Research Letters, 46, 8056–8063. https://doi.org/10.1029/2019GL083491

Yagoda-Biran, G., Hatzor, Y.H., Amit, R., & Katz, O., (2010). Constraining regional paleo peak ground acceleration from back analysis of prehistoric landslides: example from Sea of Galilee, Dead Sea transform. Tectonophysics 490, 81-91.

Youngs, R. R., Arabasz, W. J., Anderson, R. E., Ramelli, A. E., Ake, J. P., Slemmons, D. B., et al. (2003). A methodology for probabilistic fault displacement hazard analysis (PFDHA). Earthquake Spectra, 19, 191–219.

Zaslavsky, Y. (2009). Site effect and seismic hazard microzonation across the town of Tiberias, GSI Report No 502/416/09. http://mapi.gov.il/earthquake/documents/tiberias-09.pdf

Zilbermann, E., Amit, R., Bruner, I., & Nahmias, Y. (2004). Neotectonic and paleoseismic study – Bet She'an Valley: Report GSI/15/04 http://www.gsi.gov.il/Eng/_Uploads/52bet_shean_paleo.pdf

Zingboym O. & Hartal, M. (2011). Tiberias, preliminary report, Hadashot Arkheologiyot 123 http://hadashotesi.org.il/report_detail_eng.aspx?id=1821&mag_id=118

Zohar, M., Salamon, A., & Rubin, R. (2016). Reappraised list of historical earthquakes that affected Israel and its close surroundings. J Seismol, 20(3), 971-985.

Zohar, M. (2019). Temporal and Spatial Patterns of Seismic Activity Associated with the Dead Sea Transform (DST) during the Past 3000 Yr. Seism. Res. Lett., doi: 10.1785/0220190124.